Fusion of Target Detection Algorithms in Hyperspectral Images

Seniha Esen Yuksel[1]*, Ahmet Karakaya[1]

Abstract: Target detection in hyperspectral images is important in many applications including search and rescue operations, defence systems, mineral exploration and border security. For this purpose, several target detection algorithms have been proposed over the years, however, it is not clear which of these algorithms perform best on real data and on sub-pixel targets, and moreover, which of these algorithms have complementary information and should be fused together. The goal of this study is to detect the nine arbitrarily placed sub-pixel targets, from seven different materials from a 1.4km altitude. For this purpose, eight signature-based hyperspectral target detection algorithms, namely the GLRT, ACE, SACE, CEM, MF, AMSD, OSP and HUD, and three anomaly detectors, namely RX, Maxmin and Diffdet, were tested and compared. Among the signature-based target detectors, the three best performing algorithms that have complementary information were identified. Finally these algorithms were fused together using four different fusion algorithms. Our results indicate that with a proper fusion strategy, five of the nine targets could be found with no false alarms.

1. Introduction

Hyperspectral imaging (HSI) refers to the imaging of the environment with the goal of identifying the materials in each pixel based on their reflection characteristics of the sunlight. These reflection characteristics, when plotted against the wavelength, form the fingerprints of each material, and are called as the material's spectra. Using this spectral information, some of the most common applications of HSI involve the imaging of the small targets from higher altitutes [1, 2]. Such applications include save and rescue operation, target detection in defence, mineral exploration, border security as well as many others [3- 8]. Typically, hyperspectral images are collected from air-borne sensors and have low spatial resolutions [9-11]. This constitutes a problem when two or more materials fall into a single pixel. These targets are called as sub-pixel targets as illustrated in Figure 1. As these materials would have different reflection characteristics, they are not easy to identify with spectral matching methods [12, 13]. In these cases, it is helpful to fuse together several spectral matching methods and combine their strengths. On the other hand, when a vast area is of concern, it may not be practical to search every pixel to see if they match the target we are looking for. In such cases, it may be best to perform anomaly detection and to identify those pixels that are different from their surroundings first [13-17].

For target detection from spectral matching, several algorithms exist in the literature. The most popular ones include the Generalized Likehood Ratio Test (GLRT) [18-22], Adaptive Coherence Estimator (ACE) [21-22], Signed Adaptive Coherence Estimator (SACE) [21], Constrained Energy Minimization (CEM) [25, 26], Matched Filter (MF) [27], Adaptive Matched

Subspace Detector (AMSD) [26, 27], Orthogonal Subspace Projection (OSP) [27] and the Hybrid Unstructured Detector (HUD) [28, 29]. These algorithms take a known target spectra and compare it to all the pixels in the search image.
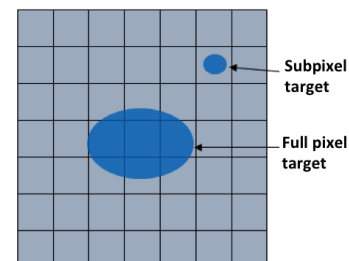

Figure 1. Subpixel and full pixel targets. A subpixel target refers to the case when more than one material is imaged by the camera in a single pixel, due to the low spatial resolution. The rest of the pixel is occupied by other materials.

On the other hand, for anomaly detection, most algorithms assume a homogenous neighbourhood and look for the pixel that deviates significantly from this neighbourhood. Arguably, the most popular of the anomaly detection algorithms is the Reed-Xiaoli (RX) algorithm [30] and most other algorithms are variants of the RX [31-33]. Two other algorithms that are worth mentioning that are not variants of RX, and thus carry complementary information are DIFDET [34] and MAXMIN [4]. Despite the large variety of spectral matching and anomaly detection papers in the literature [35-38], it is not clear which ones perfom best, especially on sub-pixel data, and which ones are complementary and worth fusing. In this paper, we make a comprehensive analysis and compare all of these methods on a real hyperspectral dataset that has nine sub-pixel targets.

In the rest of the paper, first we give the details of the dataset in Sec. 2. Then, we give details on the spectral matching algorithms in Sec. 3 and on anomaly detectors in Sec. 4. Then, we list the

[1] *Hacettepe University, Department of Electrical and Electronics Engineering, Ankara, Turkey.*
* Corresponding Author: Email: eyuksel@ee.hacettepe.edu.tr

results of these target and anomaly detectors in Sec 5. We investigate which spectral matching algorithms work best on sub-pixel targets, and which of them have complementary information. Finally, we give the details of the fusion algorithms, namely matched filter fusion, hybrid fusion, sum and product fusion in Sec. 6 and compare all the algorithms. In addition, we investigate if doing an anomaly detection before spectral matching is worth pursuing in terms of time and accuracy; and fuse the results of anomaly detection with spectral matching algorithms. In Figure 2, we show the overview of these algorithms. We then conclude the study in Sec. 8 with our findings on which algorithms to use and to fuse.
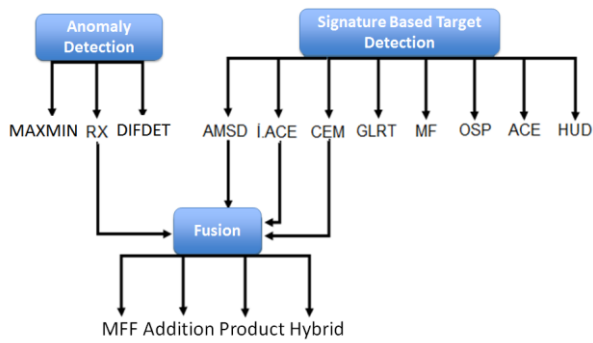

Figure 2. The algorithms tested and fused for target detection.

## 2. Hyperspectral Dataset Used in the Experiments

Hyperspectral data were collected by the Rochester Institute of Technology over the region of Chooke City, Montana, USA; using a HyMap sensor controlled with HyVista in 2006 July [39]. Nine targets from seven different materials were placed around town. Target locations and reflectance signatures of the targets were provided with the dataset [40, 41]. An aerial photograph of the area is shown in Figure 3 with a white box that shows the region of interest which includes all the targets. In Figure 3(b), locations of the targets are given superimposed on the false-color hyperspectral image, formed from the 30, 50 and 70th bands.

The collected data has 3meter spatial resolution and has 126 bands between 453 nm and 2496 nm. The water absorbtion bands, correspond to the bands between 1356-1417nm, 1820-1932nm and above 2395nm, were cropped from the image as they do not contain meaningful information for target detection [2]. After these manipulations, the data of size 145 x 350 pixels and 107 bands were used for the detection.

The target materials and sizes are given in Table 1. Only F1 and F2 materials are large enough to fully fit into a pixel; although not guaranteed. The rest of the targets are all smaller than the 3m pixel resolution; therefore, all targets can be considered as subpixel targets. The lab spectra of the targets are given in Figure 4. These were measured on the ground with a Fieldspec Pro. It can be seen that despite their color differences, targets F2 and F4 are both made from nylon, have similar spectral characteristics. Also, F1 and F3 are spectrally similar despite a shift, and differ in the red and blue color region of the spectra. Note that red color occurs around 650nm, and blue color occurs around 475nm.


(a)
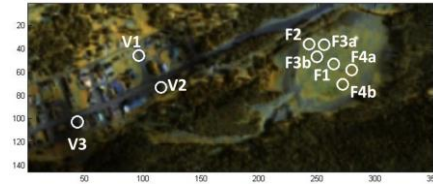
(b)

Figure 3. The photograph of the area imaged. (a) The white box shows the area that is being analysed [28]. (b) Locations of the targets on the false-color hyperspectral image.

Table 1. Properties of the Targets

Target	Dimensions (m)	Type
F1	3 x 3	Red cotton
F2	3 x 3	Yellow nylon
F3a	2 x 2	Blue cotton
F3b	1 x 1	Blue cotton
F4a	2 x 2	Red nylon
F4b	1 x 1	Red nylon
V1	4 x 2	1993 Chevy Blazer
V2	3 x 1.7	1997 Toyota T100
V3	4.5 x 1.6	1985 Subaru GL Wagon
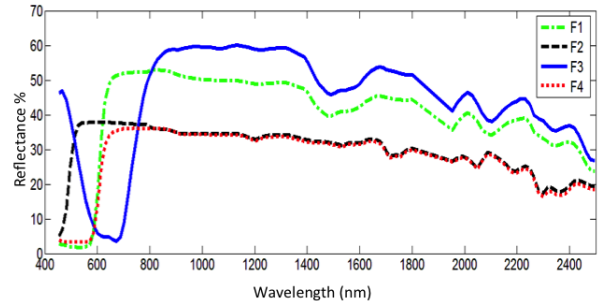
(a)
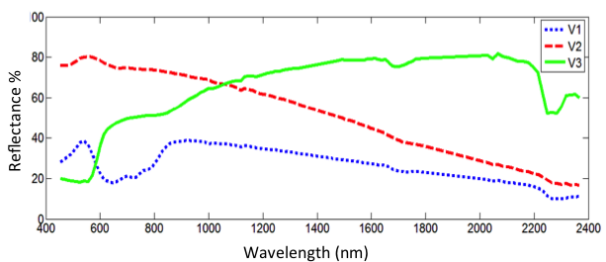
(b)

Figure 4. Spectra of the target materials

3. Signature–based Target Detection Methods

Signature-based target detection methods aim to find the target by comparing the image spectra to a known target spectra. In this section, we describe the GLRT, ACE, Signed ACE, MF, CEM, AMSD, OSP and HUD target detection methods. In our case, the known target spectra would be lab spectrum of the materials as

given in Fig. 4.

3.1. GLRT

GLRT target detection method assumes that the background, denoted as v, can be modelled with a Normal distribution. Let S be the target spectral signatures. Then the hypothesis are as follows: [18-22]

$$H_0 : \mathbf{x} = \mathbf{v} \qquad \text{not a target}$$

$$H_1 : \mathbf{x} = \mathbf{S} + \mathbf{v} \qquad \text{target}$$

Then, the GLRT score can be computed as:

$$D_{GLRT}(x) = \frac{\left[(\boldsymbol{S} - \mu)^T \hat{\boldsymbol{\Gamma}}^{-1}(\boldsymbol{x} - \mu)\right]^2}{\left[(\boldsymbol{S} - \mu)^T \hat{\boldsymbol{\Gamma}}^{-1}(\boldsymbol{S} - \mu)\right].\left[1 + \left(\frac{1}{M}\right).(\boldsymbol{x} - \mu)^T \hat{\boldsymbol{\Gamma}}^{-1}(\boldsymbol{x} - \mu)\right]} \quad (1)$$

where M is the number of pixels, μ is the mean of the backgroud and $\hat{\boldsymbol{\Gamma}}$ is the covariance of the background. If D_{GLRT} is bigger than a specified threshold, then H1 is satisfied, meaning the tested pixel x is a target; otherwise H0 is satisfied and the tested pixel is not a target.

GLRT can be used as a subpixel target detector; however, it assumes that the background covariance is the same for both hypothesis, which may not be the ideal assumption and could be very restrictive. Therefore, several extensions to GLRT relax this assumption that we briefly summarize below.

3.2. ACE

ACE is an extension to GLRT that assumes different backgrounds for the hypothesis as follows [21, 22]:

$$H_0 : \mathbf{x} = \mathbf{v} \qquad \text{nontarget}$$

$$H_1 : \mathbf{x} = \mathbf{S} + \boldsymbol{\sigma}\mathbf{v} \qquad \text{target}$$

With this, the ACE target detector can be computed as:

$$D_{ACE}(x) = \frac{\left[(\boldsymbol{S} - \mu)^T \hat{\boldsymbol{\Gamma}}^{-1}(\boldsymbol{x} - \mu)\right]^2}{\left[(\boldsymbol{S} - \mu)^T \hat{\boldsymbol{\Gamma}}^{-1}(\boldsymbol{S} - \mu)\right].\left[(\boldsymbol{x} - \mu)^T \hat{\boldsymbol{\Gamma}}^{-1}(\boldsymbol{x} - \mu)\right]} \quad (2)$$

D_{ACE} equals its maximum value when $\mathbf{x} = \mathbf{S}$, meaning the tested pixel is the target and its minimum value when $\mathbf{x} = \boldsymbol{\mu}$, meaning the tested pixel is the background.

3.3. SACE

Signed ACE (SACE) is an extension to ACE that takes into account if the target is emissive or absorbant. In this case, the sign of $(\boldsymbol{x} - \mu)^T \hat{\boldsymbol{\Gamma}}^{-1}(\boldsymbol{x} - \mu)$ is important, and the SACE detector is computed as [21]:

$$D_{SACE}(\boldsymbol{x}) = sign\left[(\boldsymbol{x} - \mu)^T \hat{\boldsymbol{\Gamma}}^{-1}(\boldsymbol{x} - \mu)\right].D_{ACE}(\boldsymbol{x}) \quad (3)$$

3.4. MF

MF is a simplified version of GLRT that also assumes that the background covariances are the same for target and nontarget pixels. MF is computed as [27]:

$$D_{MF}(\boldsymbol{x}) = \frac{(\boldsymbol{S} - \mu)^T \hat{\boldsymbol{\Gamma}}^{-1}(\boldsymbol{x} - \mu)}{(\boldsymbol{S} - \mu)^T \hat{\boldsymbol{\Gamma}}^{-1}(\boldsymbol{S} - \mu)} \quad (4)$$

3.5. CEM

CEM is a bit different from the other methods in that, it uses a finite impulse response filter to suppress the energy of the background [25, 26, 43]. The filter is of the form:

$$\boldsymbol{y}(n) = \boldsymbol{w}^T \boldsymbol{x}(n)$$

and hence the energy at the end of the filter is:

$$E = \frac{1}{N} \sum_{n=1}^{N} \boldsymbol{y}^2(n)$$

If this energy is minimized with a constraint that $\boldsymbol{w}^T \mathbf{S}$=1, the CEM target detector is obtained as:

$$D_{CEM}(x) = \frac{\boldsymbol{S}^T \hat{\mathbf{R}}^{-1} \boldsymbol{x}}{\boldsymbol{S}^T \hat{\mathbf{R}}^{-1} \boldsymbol{S}} \quad (5)$$

where $\hat{\boldsymbol{R}}$ is the correlation matrix. The correlation matrix might be preferred for faster and easier computations when the matrices get too large to handle.

3.6. AMSD

Different from all the other methods discussed so far, AMSD considers the abundances and the endmembers of the background. Let **B** be these endmembers and $\mathbf{a_b}$ be the abundances of these endmembers. In this case, the hypothesis are as follows:

$$H_0 : \mathbf{x} = \mathbf{B}\mathbf{a}_b + \mathbf{v} \qquad \text{nontarget}$$

$$H_1 : \mathbf{x} = \mathbf{S} + \mathbf{B}\mathbf{a}_b + \mathbf{v} \qquad \text{target}$$

With these hypothesis, the AMSD target detector is defined as:

$$D_{AMSD}(x) = \frac{\boldsymbol{x}^T (\boldsymbol{P}_B^\perp - \boldsymbol{P}_Z^\perp)\boldsymbol{x}}{\boldsymbol{x}^T \boldsymbol{P}_Z^\perp \boldsymbol{x}} \quad (6)$$

where **E** is a matrix that includes all the endmembers of the background and the target, and

$$\boldsymbol{P}_B^\perp = \boldsymbol{I} - \boldsymbol{B}(\boldsymbol{B}^T \boldsymbol{B})^{-1} \boldsymbol{B}^T$$

$$\boldsymbol{P}_Z^\perp = \boldsymbol{I} - \boldsymbol{E}(\boldsymbol{E}^T \boldsymbol{E})^{-1} \boldsymbol{E}^T$$

Here $\boldsymbol{P}_B^\perp$ and $\boldsymbol{P}_Z^\perp$ are the orthogonal subspace projections the matrices onto their pseudoinverses.

3.7. OSP

OSP is also like AMSD, but it only uses the endmember matrix of the background, **B** [27], and simply computes:

$$D_{OSP}(x) = \frac{\boldsymbol{S}^T \boldsymbol{P}_B^\perp \boldsymbol{x}}{\boldsymbol{S}^T \boldsymbol{P}_B^\perp \boldsymbol{S}} \quad (7)$$

3.8. HUD

HUD, like ACE, assumes different background hyphothesis, and is computed as follows [28, 29]:

$$D_{HUD}(x) = \frac{\boldsymbol{x}^T \hat{\boldsymbol{\Gamma}}^{-1} \boldsymbol{S}\hat{\boldsymbol{a}}}{\boldsymbol{x}^T \hat{\boldsymbol{\Gamma}}^{-1} \boldsymbol{x}} \quad (8)$$

where;

$$\hat{\boldsymbol{a}} = (\boldsymbol{E}^T \hat{\boldsymbol{\Gamma}}^{-1} \boldsymbol{E})^{-1} \boldsymbol{E}^T \hat{\boldsymbol{\Gamma}}^{-1} \boldsymbol{x} - (\boldsymbol{E}^T \hat{\boldsymbol{\Gamma}}^{-1} \boldsymbol{E})^{-1} \boldsymbol{\lambda}$$

$$\boldsymbol{\lambda} = \boldsymbol{E}^T \hat{\boldsymbol{\Gamma}}^{-1}(\boldsymbol{x} - \boldsymbol{E}\hat{\boldsymbol{a}})$$

which are iterated to meet the Kuhn-Tucker conditions.

4. Anomaly Detection Methods

The eight target detectors listed above are based on comparing a lab-measured signature to all the pixels in the image and seeing which ones fit most. An alternative to these methods, as described

in this section, would be to find which pixels differ most from the background. These would result in many false alarms, but were considered to see if they would decrease the false alarm rates during fusion by providing complementary information.

Three anomaly detection methods were tested; the Reed-Xiaoli (RX) [31], maximum-minimum detector (MAXMIN) [4] and the differential detector (DIFDET) [34]. The goal of these methods is to find to pixels that are different than the background. Unlike the signature-based methods, anomaly detection algorithms may be able to find all the targets at once, as they are not looking for a specific target.

4.1. RX

RX algorithm is arguably the most well-known method for anomaly detection. It puts a window on the pixel being tested as shown in Figure 5. The inner window is used as a buffer region and the part between the inner and the outer windows is used as an estimate of the background. Hence, if the pixel being tested is different than the background, it is considered as an anomaly. RX is computed as:

$$D_{RX}(\pmb{x}) = (\pmb{x} - \mu)^T \hat{\Gamma}^{-1}(\pmb{x} - \mu) \tag{9}$$

where the mean and the covariance are estimated from the background. For each pixel, the window is slided and the anomaly value is computed. In practice, to have a nonsingular solution, the outer window should have as many pixels as 10 times the number of bands.
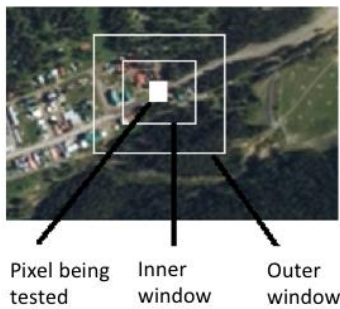
Figure 5. RX anomaly detector

4.2. MAXMIN

In the Maxmin method, the image bands are divided into two as shown in Figure 6. Then, the extremities in each region is found as:

MaM_i = Matrix of maximum spectral values for the ith subimage.

MiM_i = Matrix of minimum spectral values for the ith subimage.

MaA_i = The average of maximum spectral values for the background in the ith subimage.

MiA_i = The average of minimum spectral values for the background in the ith subimage.

and the following anomaly detector value is computed:

$MaxMin_i$ = | $MaM_i[p,q]$ - MaA_i|+ | $MiM_i[p,q]$ - MiA_i|, i = 1,2

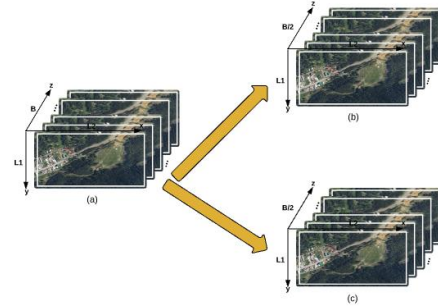Here, p and q are the coordinates of the test pixel, i stands for the subimage.

Figure 6. Maxmin method divides the images into two. For an LxKxD image, there are two hyperspectral images of size LxKxD/2.

Maxmin is a very fast method that requires only finding 4 extreme values. However, our experiments show that these extremities may not always be reliable.

4.3. DIFFDET

In the Diffdet method, the average spectrum in the local neighbourhood of a test pixel is computed. The sum of the absolute difference in each band between the test pixel's spectrum and its neighbourhood average is considered as the detector response. If the detector response exceeds a threshold value, the pixel is considered an anomaly.

5. Results of Target Detection

In this section, we provide the anomaly detection results on the Chooke City dataset, followed by the results of signature-based target detection methods.

5.1. Anomaly detection results:

For anomaly detection, we test all the 3 detectors, namely the RX, Maxmin and Diffdet, using increasing window sizes. Since all of our targets are subpixel (or at most 1 pixel), the inner window size was selected as 3 for all methods, and only the outer window size was varied. As stated before, in a single run of the algorithm, all of the targets can be searched for, as the anomaly detection methods are not looking for a specific target.

The receiver operating characteristic (ROC) curves are given in Figure 7. In the ROC plots, x-axis shows the probability of false alarm (PFA) and the y-axis shows the probability of detection (PD). Ideally, we would like to have the PFA to be zero and the PD to be one. Therefore, the closer the line to the left upper part, the better the algorithm is. Based on this information, RX can be said to operate best at a window size of 25, Maxmin at 11, and Diffdet at 45.
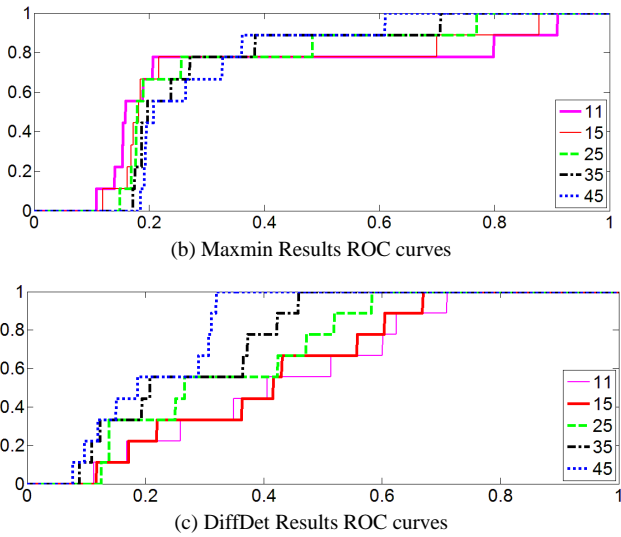
(a) RX Results ROC curves

(b) Maxmin Results ROC curves
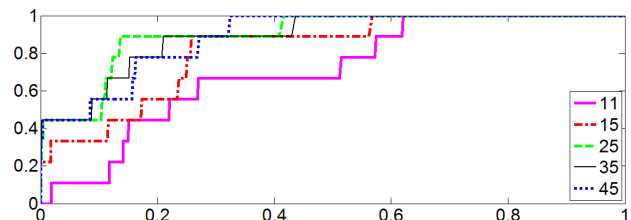
(c) DiffDet Results ROC curves

Figure 7. Anomaly Detection Results. The y-axis shows the probability of detection whereas the x-axis shows the probability of false alarm.

If we fix the PD at 80%, the FAR values are given in Table 2. The minimum value in the table is shown in bold: with 14% false alarm rates, RX algorithm with window size 25 performs the best. However, this comes with an expensive execution time as shown in Table 3. Despite its common use, it was found that RX execution time was the largest among the three detectors, and increased significantly based on the window size. This is due to the covariance matrix, which gets harder to invert, as it gets larger.

Table 2. False Alarm Rates of Anomaly Detection Algorithms when the Positive Detection Rate is 80%.

Window Size	RX	MAXMIN	DIFDET
11	0.58	0.81	0.62
15	0.25	0.70	0.60
25	**0.14**	0.47	0.53
35	0.21	0.38	0.42
45	0.27	0.35	0.32

Table 3. Execution times of the anomaly detection algorithms in seconds, with respect to increasing window sizes.

Window Size	11	15	25	35	45
RX time: (sn)	1302	1667	4504	7110	10514
MAXMIN time (sn):	2.47	2.47	2.66	3.34	3.50
DIFDET time (sn):	8	12	26	60	67

5.2. Results of Signature-based Target Detection

Using the signature-based target detection methods, only one target can be tested at a time. This makes these ROC curves have only one jump corresponding to finding/not finding the target. Therefore, a better way to describe these the success of these algorithms may be to list the number of false alarms when the target is first detected. One can think of this as the optimal threshold where the algorithm would find the target and give the least number of false alarms. Out of 50750 pixels in the image, the number of false alarms when the optimal threshold value is selected is given in Table 4.

Table 4. Number of False Alarms using the Signature-based Target Detection Algorithms

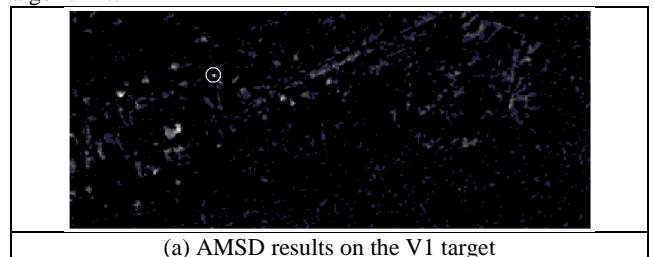| Target/Alg.	Number of False Alarms when the Optimal Threshold Value is Selected							
	GLRT	ACE	SACE	CEM	MF	AMSD	OSP	HUD
F1 (3mx3m)	0	0	0	0	0	0	0	4
F2 (3mx3m)	513	537	342	0	1	0	109	722
F3a (2mx2m)	29	33	24	8	9	0	186	50
F3b (1mx1m)	2980	2998	1851	348	1026	135	1924	2914
F4a (2mx2m)	13	13	13	1	1	0	29	47
F4b (1mx1m)	4195	4265	2490	94	468	15695	4095	1230
V1 (4mx2m)	6506	6542	3733	93	1328	3	382	506
V2 (3mx1.7m)	2631	2639	1652	30368	1342	6064	4600	570
V3 (4.5mx1.6m)	38	42	28	582	160	37	907	23

Looking at the results, the best scores on the cloth targets were detected with AMSD. When the cloth targets are bigger than 2mx2m, AMSD could perform with no false alarms. On the other hand, GLRT and ACE had similar performances; and SACE always had a better performance than ACE. This makes sense as SACE is basically ACE, but also considers if the material is an absorbing or emitting type; and both ACE and SACE are extensions to the GLRT algorithm.

In addition, we analyzed where each algorithm gave their false alarms in the image. It was seen that the following groups of algorithms gave the false alarms in the similar parts of the images:

- Group 1: AMSD, OSP and HUD
- Group 2: GLRT, ACE and SACE
- Group 3: CEM and MF

Among these groups, AMSD, CEM and SACE stood out as the better of the eight algorithms. In addition, based on where they gave false alarms, they were seen to complement each other. One example is shown in Figure 8 for target V1. The white circles show the location of the target. The other grayscale points are the false alarms, where a bright value indicates a higher score of the target detection algorithm. It can be seen that most false alarms are occurring at different places, giving an indication that these three algorithms are good to fuse together. In Figure 8, AMSD is giving more false alarms on the upper right corner, CEM is giving more false alarms on the lower left corner and SACE is giving more false alarms to the bottom right corner.

Also, in Table 5, we show the number of false alarms common to all three algorithms. It can be seen that under a good threshold value, these three algorithms complement each other nicely, and lead to zero false alarms for most targets. For this reason, in the next section, we investigate methods for the fusion of these three algorithms.
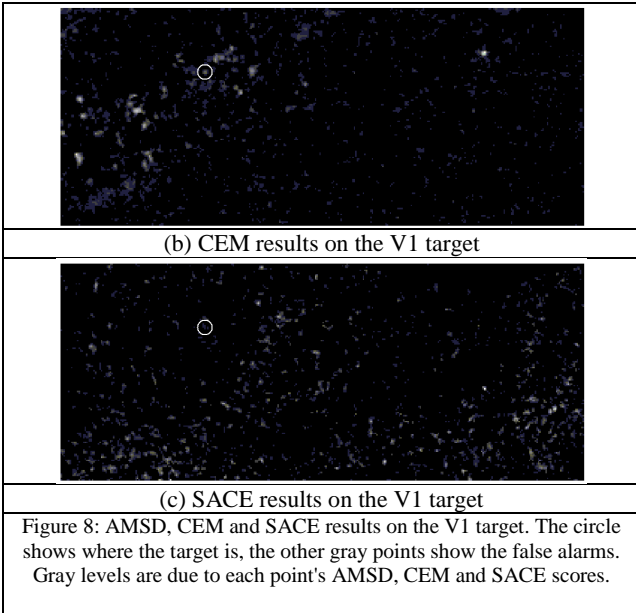

(a) AMSD results on the V1 target

(b) CEM results on the V1 target

(c) SACE results on the V1 target

Figure 8: AMSD, CEM and SACE results on the V1 target. The circle shows where the target is, the other gray points show the false alarms. Gray levels are due to each point's AMSD, CEM and SACE scores.

Table 5. Number of false alarms that are common to SACE, CEM and AMSD.

Target	Number of False Alarms Common to All Three Algorithms			
	SACE	CEM	AMSD	Common
F1	0	0	0	0
F2	342	0	0	0
F3a	24	8	0	0
F3b	1851	348	135	2
F4a	13	1	0	0
F4b	2490	94	15695	64
V1	3733	93	3	0
V2	1652	30368	6064	93
V3	28	582	37	0

6. Fusion Methods

In this study, it was seen that none of the anomaly detectors or the signature-based detectors could reach 100% detection. Therefore, to combine all these algorithms in the best possible way, the multiplication, summation [10], hybrid fusion [44] and matched filter fusion (MFF) [45- 47] methods that excel in the literature, were tested. Below, we briefly explain these methods and give the results of fusion.

6.1. MFF

MFF aims to increase the signal-to-noise ratio (SNR) of the targets by bringing together the output of the detection algorithms. Let $\mathbf{r}_i$ be the ouput of the ith algorithm. For n algorithms, the matrix R can be arranged as follows:
$$R = [r_1, r_2 \dots r_n]^T$$
Then, the target vector t can be formed by listing the maximum values of the detectors as follows:
$$t = [\max(r_1), \max(r_2), \dots \max(r_n)]^T$$
And the result of the MFF output can be computed as:

$$f_{MF} = (R - M)^T K^{-1}(t - m) \qquad (9)$$
where m is the column vector that represents the mean of the R matrix, and K is the covariance matrix of R. Also, M represents the matrix whose columns are all m.

6.2. Hybrid fusion

The hybrid fusion algorithm depends on the number of pixels that exceeds the score value of the test pixel. Let D_{Det1} and D_{Det2}

be the outputs of the algorithms to fuse. Hybrid fusion works as follows:

1. Compute N_{DET1}, the number of pixels in the image that satisfy $D_{Det1}(x) \geq D_{Det1}(x_i)$ where x_i is the test pixel.
2. Compute $n_{Det1+Det2}$, the number of pixels in the image that satisfy both $D_{Det1}(x) \geq D_{Det1}(x_i)$ and $D_{Det2}(x) \geq D_{Det2}(x_i)$.
3. Compute $r(x_i) = \frac{n_{Det1+Det2}}{N_{Det1}}$.
4. Compute the output of the hybrid detector as $D_{HYBRID}(x_i) = r(x_i) \cdot D_{Det1}(x_i)$.

Finally, the last two methods, product and sum fusion, simply multiply or sum the outputs of the target detectors.

6.3. Fusion Results

As stated before, AMSD, CEM and SACE algorithms were selected from signature-based target detection; and RX was selected from anomaly detection for fusion. Before the fusion algorithms are applied, all the outputs of the target detectors were normalized to be between 0-1, so that no detector dominates the fusion.

Two of the ROC curves resulting from the fusion are given in Figure 9 and Figure 10 for targets F3 and V3. Since there are two F3 targets, the ROC is a staircase; and since V3 is a single target, there is only one jump, indicating the target has been found. Considering both of the F3 targets and only the CEM and SACE algorithms, MFF fusion of CEM and SACE results in the best detection rates in Figure 9. (Note that the colors might be overlapping). Figure 10, shows a zoomed version of the ROC curve, therefore, the algorithms that did not perform well were cropped (which would be at the right upper corner of the figure). If only CEM and SACE fusion is considered, among the other alternatives, the product of SACE and CEM gives the best fusion results and significantly shifts the ROC curve from the right (green line) to the left (blue line).
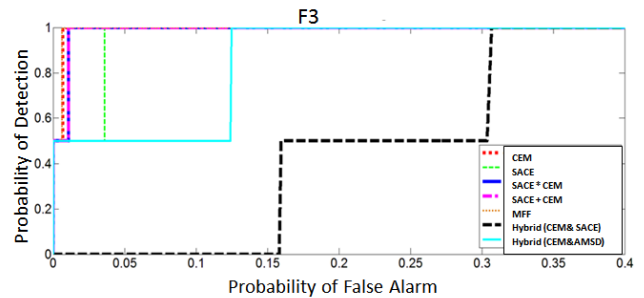

Figure 9. Sample fusion results for target F3, considering only the fusion of CEM and SACE.
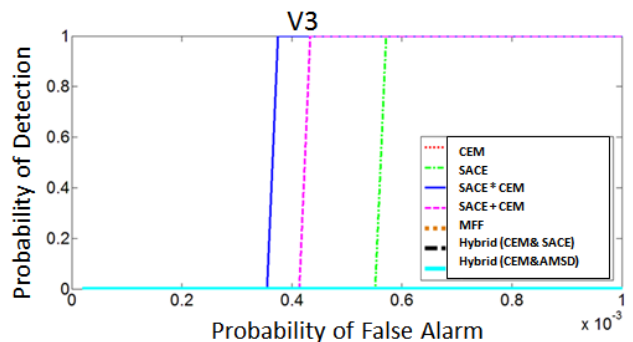

Figure 10. Sample fusion results for target V3, considering only the fusion of CEM and SACE.

If all three algorithms are tested, and if we record the percentage of false alarms at the time when detection has occurred, Table 6 is obtained. Here, the best performing algorithms for each target (in each column) is shaded in red, and the second best performing algorithm for each target is shaded in green. In this table, if we examine each row, it can be observed that fusing three algorithms always performs better than fusing two algorithms, which is better than no fusion at all. However, it is also seen that the RX, an anomaly detector had the worst results when it is run alone, as expected, but also did not contribute to the fusion in general. If we count the number of green and red cells in each row, it can be observed that the product of CEM, SACE and AMSD provides the best results.

Table 6. Percentage of false alarms from the fusion of SACE and CEM

Algorithms/Targets	F1	F2	F3a	F3b	F4a	F4b	V1	V2	V3
CEM	0	0	0.015	0.70	0.008	0.20	0.17	62	1.10
SACE	0	0.7	0.045	3.50	0.024	4	8	8	0.054
AMSD	0	0	0	0.27	0	31	0.02	12	0.062
RX	0.008	0.06	0.4	16	0.080	8	11	32	37
Sum CEM & SACE	0	0.005	0	1.10	0.010	0.56	0.50	26	0.042
Product CEM & SACE	0	0.005	0	1.10	0.010	0.40	0.85	26	0.038
MFF CEM & SACE	0	0	0	0.60	0.010	0.20	0.21	42	0.210
Hybrid AMSD & CEM	0	0.028	0.010	12	0.230	65	3	7	17
Hybrid SACE & CEM	0	42	16	30	0.220	33	53	4	19
Sum (CEM, SACE, AMSD)	0	0	0	0.10	0	0.6	0	14	0.002
Product (CEM, SACE, AMSD)	0	0	0	0.05	0	18	0	10	0.002
MFF CEM, SACE & AMSD	0	0	0	0.11	0	0.9	0	17	0.015
Sum (RX, CEM, SACE, AMSD)	0	0	0	0.14	0.008	0.6	0.01	12	0.001
Product (RX, CEM, SACE, AMSD)	0	0	0	0.18	0.010	8	0.05	8	0.008

7. Conclusion

In this study GLRT, ACE, SACE, MF, CEM, AMSD, OSP and HUD signature-based target detection methods are tested and compared on the Chooke City dataset on all the nine targets. Among these, SACE, CEM and AMSD were found to be the better-performance algorithms, and AMSD showed the best performance. In fact, AMSD showed a good performance especially if the sub-pixel target area was close to at least half of the pixel area. However, AMSD requires to model the background endmembers, which increases the computational complexity.

With this study, it was shown that AMSD, SACE and CEM showed success and weaknesses on different regions, and complemented each other. Hence, these algorithms were fused with the sum, product, MFF and hybrid fusion methods. It was shown with ROC curves and detection tables, that the false alarm rate can be significantly decreased with the fusion of these three algorithms. In addition, specifically for this dataset, the product fusion gave the best results. With product fusion, it was shown that the F1, F2, F3a, F4a and V1 targets could be detected with no false alarms.

8. Acknowledgement

References

[1] Dimitris Manolakis, Eric Truslow, Michael Pieper, Thomas Cooley, Michael Brueggeman, "Detection Algorithms in Hyperspectral Imaging Systems: An Overview of Practical Algorithms," IEEE Signal Processing Magazine, vol. 31, no. 1, 2014.

[2] Michael Theodore Eismann, Hyperspectral Remote Sensing, 2012.

[3] B. Datt, T.R. McVicar, T.G. Van Niel, D.L.B. Jupp, J.S. Pearlman, "Preprocessing EO-1 Hyperion hyperspectral data to support the application of agricultural indexes", Geoscience and Remote Sensing, IEEE Transactions, vol. 41, no. 6, pp. 1246 - 1259, 2003.

[4] Stefania Matteoli, Marco Diani, Giovanni Corsini, "A Tutorial Overview of Anomaly Detection in Hyperspectral Images", IEEE A&E Systems Magazine, 2010.

[5] Gürcan Lokman and Güray Yılmaz. "Anomaly detection and target recognition with hyperspectral images." In 2014 22nd Signal Processing and Communications Applications Conference (SIU), pp. 1019-1022. IEEE, 2014.

[6] Seniha Esen Yuksel, Thierry Dubroca, Rolf E. Hummel, and Paul D. Gader. "Differential reflection spectroscopy: A novel method for explosive detection." Acta Phys. Pol. A 123, no. 2 (2013): 263-264.

[7] Hilal Soydan, Alper Koz, H. Şebnem Düzgün, and A. Aydın Alatan. "Oil spill determination with hyperspectral imagery: A comparative study." In 2015 23nd Signal Processing and Communications Applications Conference (SIU), pp. 2404-2407. IEEE, 2015.

[8] S. E. Yuksel, T. Dubroca, R.E. Hummel, and P.D. Gader, "An automatic detection software for differential reflection spectroscopy." In SPIE Defense, Security, and Sensing, pp. 83900B-83900B. International Society for Optics and Photonics, 2012.

[9] Dimitris Manolakis, David Marden, Gary Shaw, "Hyperspectral Image Processing For Automatic Target Detection Applications", Lincoln Laboratory Journal, 2003.

[10] David Stein, Scott Beaven, Lawrence Hoff, Edwin Winter, Alan Schaum, Alan Stocker, "Anomaly Detection from Hyperspectral Imagery", IEEE Signal Processing Magazine, 2002.

[11] Randall B. Smith, Introduction to Hyperspectral Imaging, 2010.

[12] Taylor Glenn, "Context-Dependent Detection in Hyperspectral Imagery," University of Florida, 2013.

[13] M. S. Alam, M. I. Elbakary, and M. S. Aslan. "Object detection in hyperspectral imagery by using K-means clustering algorithm with pre-processing." In Defense and Security Symposium, pp. 65740M-65740M. International Society for Optics and Photonics, 2007.

[14] Özgür Murat Polat, and Yakup S. Özkazanç. "Material clustering and band reduction in spectral libraries with unsupervised hierarchical classification methods." In 2011 IEEE 19th Signal Processing and Communications Applications Conference (SIU), pp. 1081-1084. IEEE, 2011.

[15] Emrecan Bati, Akın Çalışkan, Alper Koz, and A. Aydın Alatan. "Hyperspectral anomaly detection method based on auto-encoder." In SPIE Remote Sensing, pp. 96430N-96430N. International Society for Optics and Photonics, 2015.

[16] Erdinç Acar and Selim Aksoy. "Anomaly detection with sparse unmixing and gaussian mixture modeling of hyperspectral images." In 2015 IEEE International Geoscience and Remote Sensing Symposium (IGARSS), pp. 5035-5038. IEEE, 2015.

[17] Alp Ertürk, Davut Çeşmeci, Deniz Gerçek, Mehmet Kemal Güllü, Sarp Ertürk, Integrating Anomaly Detection to Spatial Preprocessing for Endmember Extraction of Hyperspectral Images, 2013.

[18] Tareq F. Ayoub, Alexander M. Haimovich, "Modified GLRT Signal Detection Algorithm", Aerospace and Electronic Systems, IEEE Transactions, vol. 36, no. 3, pp. 810 - 818, 2000, 2000.

[19] Cohen Yuval, August Yitzhak, Blumberg Dan G., Rotman Stanley R., "Evaluating Subpixel Target Detection Algorithms in Hyperspectral Imagery," Journal of Electrical and Computer Engineering, vol. 2012, pp. 1-15, 2012.

[20] E.J. Kelly, "Adaptive Detection in Non-Stationary Interference," 1987.

[21] Edward J. Kelly, Keith M. Forsythe, "Adaptive Detection and Parameter Estimation for Multidimensional Signal Models," 1989.

[22] Sylvia S. Shen, Xiaoying Jin, Scott Paswaters, Harold Cline, Paul E. Lewis, "A Comparative Study of Target Detection Algorithms for Hyperspectral Imagery," vol. 7334, pp. 73341W-73341W-12, 2009.

[23] Qian Du, Hsuan Ren, Chein-I Chang, "A Comparative Study for Orthogonal Subspace Projection and Constrained Energy Minimization," IEEE Transactions on Geoscience and Remote Sensing, vol. VOL 41, 2003.

[24] Nasser M. Nasrabadi, "Hyperspectral Target Detection Overview", IEEE Signal Processing Magazine, 2014.

[25] Lianru Gao, Bin Yang, Qian Du, Bing Zhang, "Adjusted Spectral Matched Filter for Target Detection in Hyperspectral Imagery", Remote Sensing, vol. 7, no. 6, pp. 6611-6634, 2015.

[26] Cohen Yuval, Dan G. Blumberg, and Stanley R. Rotman. "Subpixel hyperspectral target detection using local spectral and spatial information." Journal of Applied Remote Sensing 6.1 (2012): 063508-1.

[27] Dimitris Manolakis, Gary Shaw, "Detection Algorithms for Hyperspectral Imagery Applications," IEEE Signal Processing Magazine, 2002.

[28] Joshua Broadwater, Rama Chellappa, "Hybrid Detectors For Subpixel Targets," IEEE Transactions on Pattern Analysis and Machine Intelligence, vol. VOL 29, 2007.

[29] Joshua Broadwater, Reuven Meth, Rama Chellappa, "A Hybrid Algorithm for Subpixel Detection in Hyperspectral Imagery," 2004.

[30] Irving S. Reed, and Xiaoli Yu. "Adaptive multiple-band CFAR detection of an optical pattern with unknown spectral distribution." IEEE Transactions on Acoustics, Speech, and Signal Processing 38, no. 10 (1990): 1760-1770.

[31] D. Borghys, V. Achard, S.R. Rotman, N. Gorelik, C.Perneel, E. Schweicher, "Hyperspectral Anomaly Detection: A Comparative Evaluation of Methods", 2011.

[32] Guo-Liang Zhang, Chun-Ling Yang, "Anomaly Detection for Hyperspectral Imagery Using Analytical Fusion and RX," Journal of Information Hiding and Multimedia Signal Processing, 2014.

[33] Dirk Borghys, Ingebjorg Kasen, Veronique Achard, Christiaan Perneel, "Hyperspectral Anomaly Detection: Comparative Evaluation in Scenes with Diverse Complexity," Journal of Electrical and Computer Engineering, pp. 1-16, 2012.

[34] Mohsen Zare Baghbidi, Saeid Homayouni, "Fast Hyperspectral Anomaly Detection for Environmental Applications," Journal of Applied Remote Sensing, vol. 7, no. 1, pp. 073489, 2013.

[35] Adam Cisz, Performance Comparison of Hyperspectral Target Detection Algorithms, 2006.

[36] Bill Basener, "An automated method for identification and ranking of hyperspectral target detections." SPIE Defense, Security, and Sensing. International Society for Optics and Photonics, 2011.

[37] A. Karakaya, S.E. Yuksel. "Target detection in hyperspectral images." In 2016 24th Signal Processing and Communication Application Conference (SIU), pp. 1501-1504. IEEE, 2016.

[38] A. Zare, P. Gader, J. Bolton, S. Yuksel, T. Dubroca, R. Close, and R. Hummel. "Sub-pixel target spectra estimation and detection using functions of multiple instances." In 2011 3rd Workshop on Hyperspectral Image and Signal Processing: Evolution in Remote Sensing (WHISPERS), pp. 1-4. IEEE, 2011.

[39] Rochester Institute of Technology, Chooke City Hyperspectral Image, http://dirsapps.cis.rit.edu/blindtest/. (Accessed: April, 2016).

[40] Kerekes, John P., and David K. Snyder. "Unresolved target detection blind test project overview." SPIE Defense, Security, and Sensing. International Society for Optics and Photonics, 2010.

[41] D. Snyder, J. Kerekes I, Fairweather, R. Crabtree, J. Shive, S. Hager, "Development of a Web-based Application to Evaluate Target Finding Algorithms," Proceedings of the 2008 IEEE International Geoscience and Remote Sensing Symposium (IGARSS), vol. 2, pp. 915-918, Boston, MA, 2008.

[42] Sylvia S Shen, John P Kerekes, David K Snyder, Paul E Lewis, "Unresolved Target Detection Blind Test Project Overview," vol. 7695, pp. 769521-769521-8, 2010.

[43] Yang, Shuo, and Zhenwei Shi. "SparseCEM and SparseACE for hyperspectral image target detection." IEEE Geoscience and Remote Sensing Letters 11.12 (2014): 2135-2139.

[44] Vincent Roy, "Hybrid Algorithm for Hyperspectral Target Detection," 2010.

[45] Steven Adler-Golden, Patrick Conforti, "Robust Hyperspectral Detection with Algorithm Fusion," in IEEE International Geoscience and Remote Sensing Symposium, 2010.

[46] Broadwater, Joshua, and Rama Chellappa. "Hybrid detectors for subpixel targets." IEEE transactions on pattern analysis and machine intelligence 29.11 (2007): 1891-1903.

[47] Steven Adler-Golden, Patrick Conforti, "Robust Hyperspectral Detection with Algorithm Fusion", in IEEE International Geoscience and Remote Sensing Symposium, 2010.